Anomalous Fano Profiles in External Fields

Alejandro Zielinski,[1] Vinay Pramod Majety,[1] Stefan Nagele,[2] Renate Pazourek,[2,3] Joachim Burgdörfer,[2] and Armin Scrinzi[1,*]
[1]Physics Department, Ludwig Maximilians Universität, D-80333 Munich, Germany
[2]Institute for Theoretical Physics, Vienna University of Technology, 1040 Vienna, Austria
[3]Department of Physics and Astronomy, Louisiana State University, Baton Rouge, Louisiana 70803, USA
(Received 30 June 2015; published 10 December 2015)

We show that the external control of Fano resonances in general leads to complex Fano q parameters. Fano line shapes of photoelectron and transient absorption spectra in the presence of an infrared control field are investigated. Computed transient absorption spectra are compared with a model proposed for a recent experiment [C. Ott *et al.*, Science 340, 716 (2013)]. Control mechanisms for photoelectron spectra are exposed: control pulses applied during excitation modify the line shapes by momentum boosts of the continuum electrons. Pulses arriving after excitation generate interference fringes due to infrared two-photon transitions.

DOI: 10.1103/PhysRevLett.115.243001 PACS numbers: 32.80.Qk, 31.70.Hq

The celebrated Fano formula [1]

$$\sigma(\Delta E) = \sigma_0 \frac{|q\Gamma + 2\Delta E|^2}{\Gamma^2 + (2\Delta E)^2} \tag{1}$$

describes the modulation of the cross section of any excitation process to a continuum that is structured by a single embedded resonant state compared to the smooth background cross section σ_0 in the absence of the embedded state. Apart from the resonance width Γ and the detuning ΔE there appears the q parameter, which produces a characteristic asymmetry and—if it is real—an exact zero of the cross section. The Fano profile is one of the prominent manifestations of quantum mechanical interference in scattering. The mechanism is ubiquitous and independent of the particular nature of the transitions involved. In recent years it was proposed to control the line shape by external fields and interactions, and schemes in diverse fields of physics were experimentally realized (see the review in Ref. [2]). For a quantum dot system controlled by a time-independent magnetic field it was observed that a generalization to complex q was required to fit the control dependence of the line shape. Complex values of q result from the breaking of time-reversal symmetry by the magnetic field [3]. In contrast, in the standard Fano theory [1], applicable to time-reversal symmetric systems, q is real valued (see, e.g., Ref. [4]). A complex q has also been discussed as a signature of dephasing and decoherence in atoms [5,6] as well as in quantum dots [7] and microwave cavities [8]. More generally, a complex q is expected to appear whenever coupling to the environment or external fields turns the embedded state into a state that cannot be described by a real-valued eigenfunction.

In this Letter we show that also a time-dependent electric control field, specifically an infrared (IR) probe pulse, generates complex q parameters. Recently, the control of the line shape of transient absorption spectra (TAS) arising in a pump-probe scenario for helium was demonstrated [9]: the excitation of the $2snp$ series of doubly excited states by a short extreme ultraviolet (XUV) pulse was probed by a weak, time-delayed near-IR pulse. The modulation of TAS line shapes was described as a control of the Fano q parameter through an IR induced phase shift. Here, we present *ab initio* numerical solutions that show that TAS as well as photoelectron spectra (PES) can be characterized by complex rather than real q. For PES we expose the two main mechanisms underlying the appearance of a nonzero imaginary part of q using a generalized Fano model that includes an external control. First, we show that the phase shift discussed in Ref. [9] directly leads to complex q in PES. However, a second mechanism dominates the PES line shapes when XUV and IR pulses overlap: the free electron momenta are boosted by

$$\vec{k} \to \vec{k} + \vec{A}(t_0), \qquad \vec{A}(t_0) := -\int_{t_0}^{t_1} d\tau \vec{\mathcal{E}}(\tau), \tag{2}$$

from their values after an XUV excitation time t_0 until the end of the IR field $\vec{\mathcal{E}}(t)$ at time t_1. (Unless indicated otherwise, we use atomic units, where the electron mass, proton charge, and $\hbar$ are all set equal to 1.) The boost redistributes amplitudes among the partial waves and modifies the Fano interference of the embedded state with the continuum in the $l = 1$ decay channel. Both mechanisms conserve the universal Fano line shape (1), albeit with complex q.

A higher order process that leads to a departure from the Fano profile is two-IR-photon coupling, which was discussed for a multiplet of embedded states [10] and for Autler-Townes splitting [11]. In the present setting,

two-IR-photon coupling generates characteristic interferencelike modulations of the PES when the XUV and IR pulses are well separated in time. Similar structures will appear when the decaying state is partially depleted by a delayed IR pulse [12]. The importance of nonresonant IR multiphoton processes in the excitation of dipole-forbidden autoionizing states was noted recently [13].

We first present the PES in the vicinity of the He$(2s2p)$ line as a function of the XUV excitation time t_0 with an IR pulse centered at $t = 0$ (Fig. 1). The results were obtained by numerically solving the time-dependent Schrödinger equation of the He atom in full $3 + 3$ spatial dimensions. Spectra were computed using the time-dependent surface flux method [14,15]. For a summary of the computational approach and a discussion of its accuracy, see Ref. [16]. The XUV center wavelength of $\lambda = 21$ nm was chosen to match the excitation to the $2s2p$ state, but the spectral width of ~10 eV at the pulse duration of 0.15 fs evenly covers the entire $2snp$ series of doubly excited He states. The calculations were performed for an IR wavelength of 800 nm with a pulse duration of 2 optical cycles, a peak intensity of 2×10^{12} W/cm^2, and parallel linear polarization of the XUV and IR pulses.

The two lineouts (Fig. 2) pertain to $t_0 = -3/4$ and $+1/2$ (in units of the IR optical cycle). At $t_0 = -3/4$, where the XUV pulse coincides with a node of the IR electric field, one sees a strongly asymmetric Fano profile. In contrast, at $t_0 = +1/2$, at the peak of the IR field, the profile is Lorentz-like. Neither the width nor the position of the resonance is affected by the weak IR. The pattern is repeated as t_0 is scanned through the IR pulse.

Figure 2 also contains fits to the lines by Eq. (1), where Γ was taken from the IR-free case. Only the overall intensity σ_0 and the q parameter were adjusted, either restricting q to real values and or admitting complex q, respectively. When the XUV pulse coincides with a node of the IR pulse (right

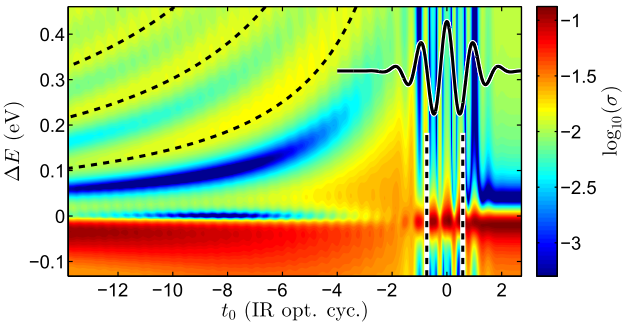

FIG. 1 (color online). PES $\sigma(\Delta E)$ in the vicinity of the $2s2p$ resonance as a function of the XUV excitation time t_0 ($l = 1$ partial wave). The IR peak intensity is 2×10^{12} W/cm^2. The solid line represents the IR field and the curved fine-dashed lines, corresponding to $2n\pi\hbar/|t_0|, n = 1, 2, 3$, closely follow the interference maxima. A negative t_0 corresponds to the XUV pulse preceding the IR pulse. The dashed vertical lines indicate the lineout times of Fig. 2.

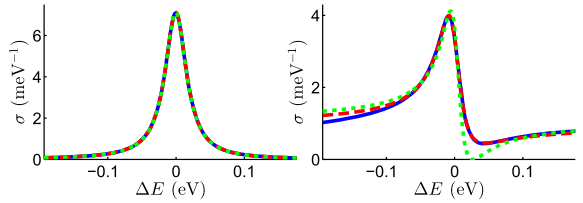

FIG. 2 (color online). PES at two different delay times as indicated in Fig. 1. Left: $t_0 = 1/2$ IR optical cycle, near a field peak. Right: $t_0 = -3/4$, near a field node. The IR peak intensity is 10^{12} W/cm^2. Solid line, numerical result; dashed line, fit admitting complex q; dot-dashed line, fit with q restricted to real. All three lines nearly coincide at $t_0 = 1/2$.

panel of Fig. 2), only the fit with complex q is satisfactory: there is no exact zero in the spectrum when the IR and XUV pulse overlap, which trivially rules out an accurate fit by Eq. (1) with real q.

For the example of PES we show how a complex q arises in the framework of a generalized Fano theory. A standard Fano Hamiltonian has the form

$$H = |\varphi\rangle E_\varphi \langle\varphi| + \int |\vec{k}\rangle \frac{k^2}{2} \langle\vec{k}| + |\vec{k}\rangle V_{\vec{k}} \langle\varphi| + |\varphi\rangle V^*_{\vec{k}} \langle\vec{k}| d^3k, \tag{3}$$

where the embedded bound state $|\varphi\rangle$ interacts with the continuum states $|\vec{k}\rangle$ through $V_{\vec{k}} = \langle\vec{k}|V|\varphi\rangle$. Solutions are known for the exact scattering eigenfunctions $|\xi_{\vec{k}}\rangle$, the resonance width Γ, and the shift of the resonance position from the noninteracting E_φ. The Fano transition amplitude $\langle\xi_{\vec{k}}|T|\phi_0\rangle$ for an arbitrary transition operator T from some initial state $|\phi_0\rangle$ leads to the Fano cross section (1). We introduce the wave packet after the transition

$$T|\phi_0\rangle = :|\psi_0\rangle = |\varphi\rangle X_\varphi + \int d^3k |\vec{k}\rangle X_{\vec{k}} \tag{4}$$

with the transition amplitudes from the initial state $X_\varphi = \langle\varphi|T|\phi_0\rangle$ and $X_{\vec{k}} = \langle\vec{k}|T|\phi_0\rangle$. For notational simplicity we consider the case where $|\varphi\rangle$ decays into a well-defined angular momentum state; in the case of the $2s2p$ doubly excited state this is the $l = 1$ partial wave. The q parameter for the standard Fano Hamiltonian (3), denoted as q_0, is

$$q_0 = \frac{1}{\pi V^*_k k} \frac{\langle\varphi|\psi_0\rangle + \mathcal{P}\int k'^2 dk' \frac{2V^*_{k'}}{k^2 - k'^2} \langle k'|\psi_0\rangle}{\langle k|\psi_0\rangle}, \tag{5}$$

where $|k\rangle$ denotes the $l = 1$ partial wave continuum state with $k = \sqrt{\vec{k}^2}$, and V_k are the coupling matrix elements between embedded and continuum states. When the $\langle k'|\psi_0\rangle$ and $\langle\varphi|\psi_0\rangle$ all share the same phase, q is real.

In our model for the transition in the pulse overlap region we assume that the initial state $|\phi_0\rangle$ is unaffected by the IR pulse and that the effect on the embedded state $|\varphi\rangle$ is only a Stark shift $\Delta E_\varphi(t)$ relative to the field-free energy E_φ. The interaction of the IR pulse with the continuum states is described in the standard "strong field approximation" [17]: when the IR field prevails over the atomic potential, the continuum states at time t can be approximated as plane waves with wave vector $\vec{k} - \vec{A}(t)$ and the phase of the time evolution is modified accordingly. Finally, we assume that the IR pulse duration is short compared to the decay time of the embedded state. With that, the net effect of the IR pulse is to replace $|\psi_0\rangle$ by a modified initial wave packet

$$|\psi_1\rangle = |\varphi\rangle X_\varphi + \int d^3k e^{-i\Phi_{\vec{k}}} |\vec{k}\rangle X_{\vec{k}-\vec{A}(t_0)} \tag{6}$$

(see the Supplemental Material [18]). The phase offset $\Phi_{\vec{k}}$ between embedded and continuum states accumulated from excitation at t_0 until the end of the IR pulse at t_1, $\vec{A}(t_1) = 0$, is

$$\Phi_{\vec{k}} = \int_{t_0}^{t_1} d\tau([\vec{k} - \vec{A}(\tau)]^2/2 - E_\varphi - \Delta E_\varphi(\tau)). \tag{7}$$

Clearly, even if the initial amplitudes X_φ and $X_{\vec{k}-\vec{A}(t_0)}$ are all real, the interaction with the IR pulse imprints a phase modulation on $|\psi_1\rangle$. Such an energy-dependent phase imprint on the initial wave packet $|\psi_1\rangle$ is generic for short-time controls. After the end of the control pulse the evolution is governed by the Fano Hamiltonian (3), but the matrix elements $\langle\varphi|\psi_0\rangle$ and $\langle k|\psi_0\rangle$ in Eq. (5) are replaced with $\langle\varphi|\psi_1\rangle$ and $\langle k|\psi_1\rangle$, which no longer share the same phase. As a result the modulated q_1 becomes complex.

For photoelectron spectra, in $X_{\vec{k}-\vec{A}(t_0)}$ in addition the partial waves are redistributed compared to the IR-free $X_{\vec{k}}$ by the addition of a streaking momentum $\vec{A}(t_0)$. A short calculation (see Ref. [18]) leads to the IR modification of the Fano parameter

$$q_1 = q_0 + a(e^{-i\chi}/\mathcal{J} - 1), \tag{8}$$

where $a = \langle\varphi|\psi_0\rangle/(\pi V_k^* k\langle k|\psi_0\rangle)$ denotes the ratio of embedded to continuum amplitudes without the IR pulse and

$$\chi = \int_{t_0}^{t_1} d\tau[\Delta E_\varphi(\tau) - \vec{A}^2(\tau)/2] \tag{9}$$

is a laser-induced phase shift between the two components. Although the phase shift χ does give a numerically discernable contribution, the t_0 dependence of q_1 is dominated by

$$\mathcal{J} = j_0(|\vec{\alpha}|k) - 2j_2(|\vec{\alpha}|k) - 3i\frac{j_1(|\vec{\alpha}|k)}{|\vec{\alpha}|k}\vec{\alpha}\cdot\vec{A}(t_0), \tag{10}$$

where the spatial offset of a free electron by the IR pulse

$$\vec{\alpha} = \int_{t_0}^{t_1} d\tau\vec{A}(\tau) \tag{11}$$

appears in the argument of the spherical Bessel functions j_l. The $\mathcal{J}$ term accounts for streaking by the term $\int_{t_0}^{t_1}\vec{k}\cdot\vec{A}(\tau)d\tau$ in $\Phi_{\vec{k}}$. By the dipole selection rule $|\psi_0\rangle$ has angular momentum $l = 1$ and therefore only the j_0, j_1, and j_2 contribute to the $l = 1$ partial wave emission.

In Fig. 3 we compare Eq. (8) with fits to the numerically computed $2s2p$ line. For the fits, the amplitude ratio was kept constant at the field-free value of $a = -3.3$ and Stark shifts were neglected, $\Delta E_\varphi \equiv 0$. Sign changes of the real part and peaks in the imaginary parts are all well reproduced. Quantitative deviations must be expected in the strong field approximation, due to the use of plane waves $|\vec{k}\rangle$ instead of the exact scattering solutions. In addition, there is a non-negligible IR two-photon coupling, as will be discussed below.

There are excitation times $t_0 = t_n$ where the spatial offset vanishes, $\vec{\alpha} = 0$, and therefore $\mathcal{J} = 1$. At these delays, the imaginary part of q_1 is exclusively due to the phase shift χ. Up to small corrections arising from the short IR pulse duration, the t_n coincide with zeros of the field. At the t_n the profile is Fano-like (Fig. 2), except that the characteristic minimum remains slightly above zero. In our model, the minima for subsequent t_n's grow monotonically as the delay $|t_0|$ increases (Fig. 3, right panel) reflecting the accumulation of the shift χ (9). For overlapping pulses, all resonances $2snp$, $n = 2$ through 7, show the same delay dependence, which corroborates that line shape modulations are dominated by the dressing of the continuum.

When the XUV pulse precedes the IR pulse without overlap (large negative t_0), the spatial offset goes to zero ($\vec{\alpha} \approx 0$) and therefore $\mathcal{J} \approx 1$. Here, the line shapes are the

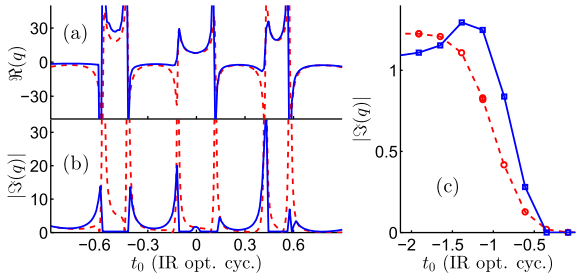

FIG. 3 (color online). Dependence of q_1 on the XUV-IR delay time t_0 according to Eq. (8) (dashed lines) and from fits to numerical results (solid lines). (a) $\Re(q_1)$. (b) $|\Im(q_1)|$. (c) $|\Im(q_1)|$ at times t_n near the nodes of the field ($\vec{\alpha} = 0$, see text) for Eq. (8) (bullets) and the fit (squares).

combined effect of the phase shift χ and IR two-photon coupling between embedded and continuum states. Two-photon coupling is not included in the standard Fano model (3). It manifests itself in sidebandlike interferences. Stimulated two-IR-photon emission creates ripples in the otherwise smooth nonresonant PES to the left of E_φ around $E_l = E_\varphi - 2\omega$, where ω is the IR photon energy. The electron amplitude generated by two-photon absorption near $E_r = E_\varphi + 2\omega$ is superimposed with the higher-lying Fano resonances and therefore is not clearly discernable. Absorption-emission transitions couple the embedded state to the continuum near $E = E_\varphi$. We model the spectral features near E_β, $\beta = \varphi, l$ by

$$\sigma(E) = |f(E) + \mathcal{E}_0^2 e^{-it_0(E-E_\beta)} b_\beta(E)|^2, \qquad (12)$$

where t_0 is the XUV-IR delay, $\mathcal{E}_0$ denotes the IR peak field strength, and $f(E)$ is the spectral amplitude in the absence of the IR pulse. The unknown two-IR-photon transition amplitudes are parametrized as $b_\beta(E) = c_\beta g(E - E_\beta)$. For g we use a Gaussian profile with a fixed width equal to the spectral width of the IR pulse. The only adjustable parameters are the two-photon coupling strengths c_β, accounting for the different strengths of the transition into a structured and unstructured continuum.

In Fig. 4 the cross section (12) at $t_0 = -12$ IR optical cycles is compared to the time-dependent Schrödinger equation result. The fringe separation of $2\pi/t_0$ discernable in Figs. 1 and 4 proves that the structures are caused by the interference of photoelectrons emitted at the relative delay t_0. Without any further adjustment of c_β or g the model equally well reproduces the spectra for varying intensities up to $I \lesssim 10^{12}$ W/cm^2 and for all t_0. The quadratic dependence on the IR field strength $\mathcal{E}_0$ shows that this is a true two-photon process without resonant coupling to neighboring states. At short time delays t_0 the effect is negligible, as fringe separation diverges and fringes are hardly discernable.

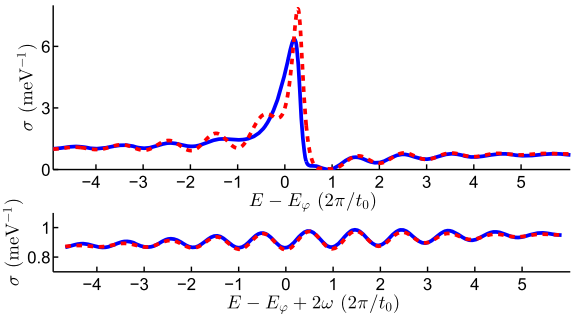

FIG. 4 (color online). Two-photon interference resonance in the $l = 1$ partial wave near E_φ (upper panel) and near $E_\varphi - 2\omega$ (lower panel). The cross section (12) (dot-dashed line) is compared to the full numerical result (solid line) at $t_0 = -12$ optical cycles.

Turning to the complementary channels for observing Fano line shape control by the IR field we calculated TAS near the $2snp$, $n \leq 6$, states using the pulse parameters of Ref. [9]. The spectra were determined from the full solutions of the time-dependent Schrödinger equation following the method described in Ref. [19].

The delay dependence of the TAS differs from that of the PES: under the influence of the IR field the characteristic minimum of the Fano line all but disappears and does not fully reappear for delays shorter than the resonance lifetime. Figure 5 shows as an example the computed transient absorption line of the $n = 4$ resonance at different IR delays. In all cases, the numerical results are accurately fitted using the field-free line parameters and adjusting complex q. A theoretical description of the TAS line shapes was given in Ref. [9], where the line is composed of a Fano profile with a modified real q_m and a pedestal that is fully determined by q_m (see the supplemental materials and Fig. S1 of Ref. [9]). Figure 5 includes the lines following the model of Ref. [9], where we use the values of q_m resulting from the main text, Eqs. (4b), (22), and (24), and the supplemental materials of Ref. [9]. The line shapes are qualitatively correct, but the predicted peaks are too high by ≈10% in Fig. 5(b) and ≈30% in Fig. 5(c). This discrepancy is inherent in the line shape given in Ref. [9] and cannot be eliminated by choosing different q_m. For an accurate reproduction of the simulated line shape, one must introduce more parameters, for example, an independent fit of the pedestal, or, as above, an imaginary part of q.

The modifications of the Fano profiles appear at parameters that are accessible by experimental setups as in Ref. [9]. For PES we predict the line shape (8). For TAS a local cross section minimum above zero provides support for the appearance of complex q or, in an alternative parametrization, real q_m with a pedestal. The main experimental difficulty is the proper background subtraction. In the case of the PES, the presence of the IR pulse

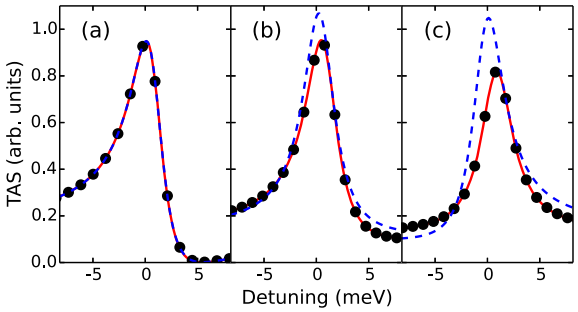

FIG. 5 (color online). TAS at the $2s4p$ resonance. Results are shown for (a) the XUV pulse only, (b) a 7 fs FWHM IR pulse with peak intensity $I = 2 \times 10^{12}$ W/cm^2 reached at arrival of the XUV pulse, and (c) the peak IR intensity 5 fs after the XUV pulse. Dots: numerical results. Red solid line: fit of a Fano profile with complex q. Blue dashed line: line shape of Ref. [9]. The lines trivially coincide in (a).

introduces a smooth background of partial waves, Eq. (2), in addition to the $l = 1$ partial wave that exhibits the Fano interference. However, at the times t_n where $\vec{\alpha} = 0$ the contributions from the other partial waves are negligible and $\Im(q)$ as given in the right panel in Fig. 3 is directly observable in the angle-integrated cross section. At other delays, the $l = 1$ cross section must be reconstructed from an angle-resolved measurement (see, e.g., Ref. [20]).

In summary, anomalous Fano profiles with a complex q parameter appear whenever a nontrivial relative phase between the embedded state and the continuum is imprinted on the system during the Fano decay. Such a phase can reflect the internal dynamics of the embedded state $|\varphi\rangle$, i.e., when it is not strictly an eigenstate of a stationary Hamiltonian, as for decaying states and decoherence. It can equally be generated by an external control, as demonstrated here. Our theoretical description of the process should be generalizable to systems where we can model the impact of the control on bound and embedded states and when the control time is short compared to the resonance lifetime. This is the case for laser pulses on atoms or molecules, but the approach is also valid, e.g., for time-dependent electric or magnetic fields acting on quantum dots.

We acknowledge support by the excellence cluster Munich Center for Advanced Photonics (MAP) and by the Austrian Science Foundation project ViCoM (F41) and NEXTLITE (F049).

*armin.scrinzi@lmu.de

[1] U. Fano, Phys. Rev. **124**, 1866 (1961).
[2] A. E. Miroshnichenko, S. Flach, and Y. S. Kivshar, Rev. Mod. Phys. **82**, 2257 (2010).
[3] K. Kobayashi, H. Aikawa, S. Katsumoto, and Y. Iye, Phys. Rev. B **68**, 235304 (2003).
[4] H.-W. Lee, Phys. Rev. Lett. **82**, 2358 (1999).
[5] G. S. Agarwal, S. L. Haan, and J. Cooper, Phys. Rev. A **29**, 2552 (1984).
[6] M. Wickenhauser, J. Burgdorfer, F. Krausz, and M. Drescher, Phys. Rev. Lett. **94**, 023002 (2005).
[7] A. A. Clerk, X. Waintal, and P. W. Brouwer, Phys. Rev. Lett. **86**, 4636 (2001).
[8] A. Bärnthaler, S. Rotter, F. Libisch, J. Burgdörfer, S. Gehler, U. Kuhl, and H.-J. Stöckmann, Phys. Rev. Lett. **105**, 056801 (2010).
[9] C. Ott, A. Kaldun, P. Raith, K. Meyer, M. Laux, J. Evers, C. H. Keitel, C. H. Greene, and T. Pfeifer, Science **340**, 716 (2013).
[10] Z. X. Zhao and C. D. Lin, Phys. Rev. A **71**, 060702 (2005).
[11] W.-C. Chu and C. D. Lin, Phys. Rev. A **87**, 013415 (2013).
[12] J. Zhao and M. Lein, New J. Phys. **14**, 065003 (2012).
[13] W.-C. Chu, T. Morishita, and C. D. Lin, Phys. Rev. A **89**, 033427 (2014).
[14] L. Tao and A. Scrinzi, New J. Phys. **14**, 013021 (2012).
[15] A. Scrinzi, New J. Phys. **14**, 085008 (2012).
[16] V. P. Majety, A. Zielinski, and A. Scrinzi, New J. Phys. **17**, 063002 (2015).
[17] M. Lewenstein, P. Balcou, M. Y. Ivanov, A. L'Huillier, and P. B. Corkum, Phys. Rev. A **49**, 2117 (1994).
[18] See Supplemental Material at http://link.aps.org/supplemental/10.1103/PhysRevLett.115.243001 for a derivation of Eq. (8).
[19] M. B. Gaarde, C. Buth, J. L. Tate, and K. J. Schafer, Phys. Rev. A **83**, 013419 (2011).
[20] G. A. Garcia, L. Nahon, and I. Powis, Rev. Sci. Instrum. **75**, 4989 (2004).